IEEE Access
Multidisciplinary ⋮ Rapid Review ⋮ Open Access Journal

Received April 20, 2018, accepted June 19, 2018, date of publication June 28, 2018, date of current version July 25, 2018.

Digital Object Identifier 10.1109/ACCESS.2018.2851284

H_∞ Control Design of PID-Like Controller for Speed Drive Systems

PO-JEN KO, (Student Member, IEEE), AND MI-CHING TSAI, (Senior Member, IEEE)
Department of Mechanical Engineering, National Cheng Kung University, Tainan 701, Taiwan

Corresponding author: Mi-Ching Tsai (mctsai@mail.ncku.edu.tw)

This work was supported by the Ministry of Science and Technology of Taiwan under Project MOST 106-2218-E-006-023.

ABSTRACT The proportional-integral-derivative (PID) controller has been widely used in industrial servo drives for its simplicity and reliability. This paper employs H_∞ control to design the PID-like controller for both velocity and current feedback loops. A dedicated design formulation is proposed such that three control parameters can be obtained directly by H_∞ control. The weighting functions involved in H_∞ control design are specified in terms of motor specifications to provide an initial design, and then the relative weights are chosen iteratively to further achieve the required performance. To reduce the effects of sensor noises and phase delay, an H_∞ observer design is formulated dually to construct a PID-like speed observer. The present approach aims to adopt modern control tools that ensure the stability of the closed-loop system to characterize the PID-like controllers such that the desired control performance can be achieved systematically. An illustrated design example is given to demonstrate the proposed design approach for both the speed controller and the observer in practice. Experimental results show that the H_∞ PID-like controller is superior to a classical cascade design in terms of disturbance rejection ability.

INDEX TERMS H_∞ control, weighting function design, PID controller, disturbance rejection.

I. INTRODUCTION

An industrial servo drive is widely adopted in robot, vehicle, metal forming machine, and laser auto-focus system applications [1]–[4]. Tuning the cascade current and velocity loops for achieving velocity control is common in servo drive design. As shown in Fig. 1, the tuning process can be started by tuning the inner loop to achieve the specified performance. Next, the outer loop is tuned for which the bandwidth of the outer loop is expected to be around 10% of that of the inner loop [5], [6].

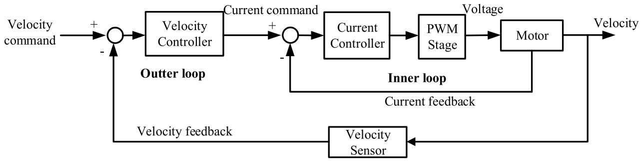

FIGURE 1. **Velocity control: two loops cascaded [5], [6].**

The classical control architecture of a servo drive is usually composed of a proportional controller P, an integral controller I, and a differential controller D. With different combinations of P, I and D, the required control objectives can be achieved. For instance, a PI controller can enhance the bandwidth and reduce the steady-state error [7]; the IP controller is modified from the ID controller [8]; the so-called pseudo derivative feedback (PDF) controller can realize an equivalent derivator to avoid the effects of noise; The PID controller is the most frequently used in many industrial applications [9]. However, the control system has inherent limitations in tracking response and stability, which leads to the challenge of controller parameter tuning for system response optimization. It is known that the PID controller tuning method was firstly proposed by Ziegler and Nichols [10]. The development of optimal control design greatly depends on optimal performance of PID controllers. For instance, an LQR approach was proposed in [11] to contribute an optimal PID controller; furthermore, Li [12] developed a PID controller tuning method based on specified gain and phase margins for a desired performance optimization; Dai *et al.* [13] applied fuzzy rules to automatically tune the proportional PID parameters.

Control engineers commonly face a challenge when implementing the abovementioned methods in that tuning high gains increases the bandwidth, but results in an unstable system. Under the consideration of both tracking performance and robust stability, the modern control approach of H_2 and/or H_∞ can be adopted to design servo drives [14]–[16]. However, the standard H_2 and/or H_∞ control problem

2169-3536 © 2018 IEEE. Translations and content mining are permitted for academic research only.
Personal use is also permitted, but republication/redistribution requires IEEE permission.
See http://www.ieee.org/publications_standards/publications/rights/index.html for more information.

formulation often obtains a high-order dynamic controller, which complicates implementation in practice.

Taking robust control design of servo drive into account, this paper proposes a PID-like controller that is based on practical implementation of the cascade structure. In contrast to the cascade control design approach of [5], this study formulates the servo controller design of the velocity loop and the current loop simultaneously. The specific state-feedback H_∞ control formulation was addressed in [17] to directly solve the constant controller parameters. However, how to select the weighting functions to obtain an appropriate robust controller is still a critical problem. As a practical approach, this paper first adopts the motor specifications in terms of weighting functions such that the chosen performance index can be normalized by the scaling factors, namely nondimensionlized. Then, the relative constant (i.e., dimensionless) weights are selected iteratively to provide design freedom for further performance improvement.

It is known that high gain control design to achieve a desired bandwidth will increase noise sensitivity. Besides, using a low-pass filter to reduce the noise has an inherent phase delay, which may lead to an unstable feedback control system. In this paper, the speed observer design presented in [18] is adopted to reduce the effects of sensor noises. The observer design is formulated purposely as a specific output-injection case of H_∞ control problems such that the controller parameters can be computed directly [17]. A DC servomotor drive design is practically implemented to show the validity of the proposed method.

II. CONTROL DESIGN SCHEMES

A. CONVENTIONAL METHOD: CLASSICAL CASCADED DESIGN

The velocity controller of a servo drive from the speed command ω^* to the controlled output ω can be achieved via classical cascade design with a proportional current controller and the so called IP velocity controller as shown in Fig. 2, where R, L, J_m, B_m, K_t, and K_e denote the motor parameters of resistance, inductance, inertia of rotor, damping ratio, torque constant, and back EMF constant, respectively. K_{cp}, K_{vp} and K_{vi} denote the current and speed controller parameters, respectively.

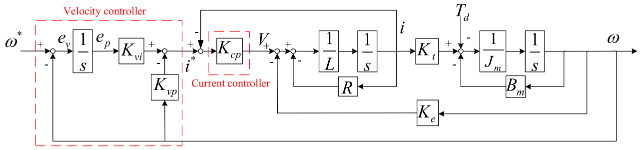

FIGURE 2. Block diagram of classical cascade design.

The proportional controller K_{cp} of the inner current loop should be designed such that the bandwidth of the current loop from the current command i^* to the controlled i is much wider than that of the velocity loop. Consider the current controller design of a DC motor as shown in Fig. 3, where the closed loop transfer function from i^* to i is given by

$$\frac{i}{i^*} = \frac{K_{cp}/L}{s + \left(R + K_{cp}\right)/L}. \tag{1}$$

Given the parameters of the DC motor depicted in Table 1, let the desired bandwidth of the current loop be 1kHz. Then, the controller gain can be found as $K_{cp} = 16.721$, which is calculated from $\left(R + K_{cp}\right)/L = 2\pi \times 1000$ in (1). For the velocity controller design, if the velocity loop bandwidth ($B.W.$) is set to 100Hz, which is 10% of the inner loop (i.e., $B.W. = 2\pi \times 100$), then the transfer function of the current loop can be approximated as a constant, $K_c = K_{cp}/(R + K_{cp})$, as shown in Fig. 4.

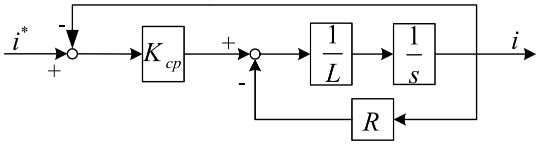

FIGURE 3. Current loop control of Fig. 2.

TABLE 1. Parameters of motor.

Symbol	Quantity	Value
R	Resistance	7.155 (Ω)
L	Inductance	0.0038 (H)
J_m	Moment inertia	5.77×10^{-5} ($kg\cdot m^2$)
B_m	Damping coefficient	0.00055 ($N\cdot m\cdot s/rad$)
K_e	Back-EMF constant	0.21 ($V\cdot s/rad$)
K_t	Torque constant	0.21 ($N\cdot m/A$)
V_R	Rated voltage	75 (V)
i_R	Rated armature current	2 (A)
ω_R	Rated speed	3000 (rpm)
T_R	Rated torque	0.34 ($N\cdot m$)
$\dot{P}_R$	Rated power rate	3400 (W/s)
K_{stiff}	Stiffness	54.993 ($N\cdot m/rad$)

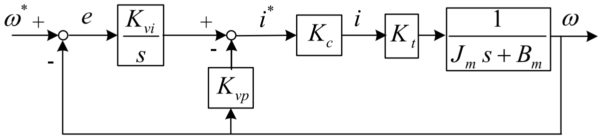

FIGURE 4. Velocity loop control of Fig. 2.

The transfer function from ω^* to ω as depicted in Fig. 4 can be expressed as

$$\frac{\omega}{\omega^*} = \frac{\frac{K_{vi}K_cK_t}{J_m}}{s^2 + \frac{(B_m+K_{vp}K_cK_t)}{J_m}s + \frac{K_{vi}K_cK_t}{J_m}} = \frac{\omega_n^2}{s^2 + 2\zeta\omega_n + \omega_n^2}, \tag{2}$$

where ω_n denotes the natural frequency of the speed control loop and ζ is the damping ratio. As can be seen from (2), this is in fact a standard second order system. By specifying the natural frequency and the damping ratio, the velocity bandwidth can be calculated from $B.W. = \omega_n(1-2\zeta^2+\sqrt{2-4\zeta^2+4\zeta^4})^{\frac{1}{2}}$. For example, letting $\omega_n = 976.26$ and $\zeta = 1$, the controller gains can be obtained as $K_{vi} = 373.93$ and $K_{vp} = 0.7623$. The resulting bandwidths of the current loop and velocity loop can be found to be 997.63Hz and 99.797Hz, respectively.

B. PROPOSED METHOD: PID-LIKE CONTROLLER DESIGN

H_∞ control design is one robust control technique to enhance stability and performance with respect to parameter variations [19], [20]. Consider the general H_∞ control design framework shown in Fig. 5, where the two-port transfer function matrix $P = \begin{bmatrix} P_{11} & P_{12} \\ P_{21} & P_{22} \end{bmatrix}$ denotes the standard control configuration (SCC) and K_∞ is the stabilizing controller to be designed [21]. The closed-loop transfer function from the input w to the output z is given by the Linear Fractional Transformation (LFT) defined by

$$LFT_l\left(\begin{bmatrix} P_{11} & P_{12} \\ P_{21} & P_{22} \end{bmatrix}, \; K_\infty\right) := P_{11} + P_{12}K_\infty(I - P_{22}K_\infty)^{-1}P_{21} \quad (3)$$

For a given pre-specified $\gamma > 0$, the H_∞ sub-optimal control problem is to find a stabilizing controller K_∞ [21] to satisfy the performance index

$$\|LFT_l(P, K_\infty)\|_\infty < \gamma \quad (4)$$

In fact, this H_∞ control problem is equivalent to solving [22]

$$\left\| LFT_l\left(\begin{bmatrix} \frac{1}{\gamma}P_{11} & \frac{1}{\gamma}P_{12} \\ P_{21} & P_{22} \end{bmatrix}, K_\infty\right) \right\|_\infty < 1. \quad (5)$$

Generally, the standard H_∞ control design problem often leads to high-order dynamic controllers [21], [22], which complicates implementation in practice. Consider the classical control architecture of Fig. 6, which is equivalent to Fig. 2, where the controller contains the proportional controller P, the integral controller I, and the differential controller D, namely PID-like controller hereafter. The PID-like controller shown in Fig. 6 can be implemented as depicted in Fig. 7, where the controller parameters can be formulated into a state-feedback (SF) design problem and then calculated directly by the H_∞ solution algorithm [23]. Note that the weighting functions W_ω, W_p, and W_V marked in the dash-line boxes are given to provide flexible design trade-off to achieve desired specifications.

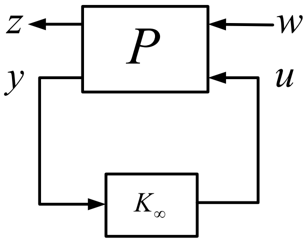

FIGURE 5. Standard formulation of controller design.

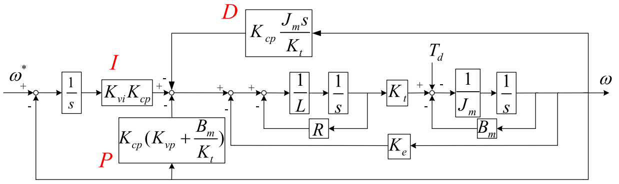

FIGURE 6. Equivalent block diagram of Fig. 2.

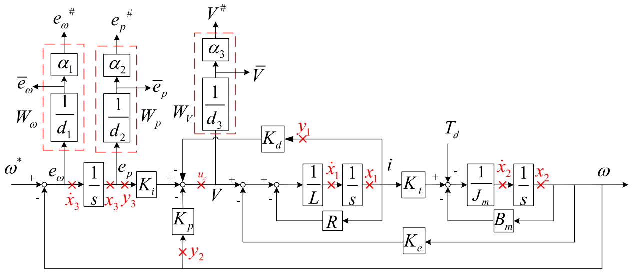

FIGURE 7. Block diagram of controlling motor with PID-like controller.

Let the state-space realization (A, B, C, D) of the SCC plant be denoted $P_c(s) = D + C(sI - A)^{-1}B$ and the weighting functions be given by $W_p = \frac{\alpha_1}{d_1}$, $W_\omega = \frac{\alpha_2}{d_2}$, and $W_V = \frac{\alpha_3}{d_3}$ to characterize the required specifications. Now consider the weighted control design problem of Fig. 7. A state-space realization of the SCC plant $P_c(s)$ can be obtained as

$$P_c(s) \overset{s}{=} \left[\begin{array}{c|cc} A & B_1 & B_2 \\ \hline C_1 & D_{11} & D_{12} \\ C_2 & D_{21} & 0 \end{array}\right] = \left[\begin{array}{ccc|cc|c} -\frac{R}{L} & -\frac{K_e}{L} & 0 & 0 & 0 & \frac{1}{L} \\ \frac{K_t}{J_m} & -\frac{B_m}{J_m} & 0 & 0 & -\frac{1}{J_m} & 0 \\ 0 & -1 & 0 & 1 & 0 & 0 \\ \hline 0 & 0 & W_p & 0 & 0 & 0 \\ 0 & W_\omega & 0 & W_\omega & 0 & 0 \\ 0 & 0 & 0 & 0 & 0 & W_V \\ \hline 1 & 0 & 0 & 0 & 0 & 0 \\ 0 & 1 & 0 & 0 & 0 & 0 \\ 0 & 0 & 1 & 0 & 0 & 0 \end{array}\right]. \quad (6)$$

As can be seen above, since $C_2 = I$ and $D_{21} = 0$, the controller inputs $\begin{bmatrix} y_1 & y_2 & y_3 \end{bmatrix}$ are in fact the system states $\begin{bmatrix} x_1 & x_2 & x_3 \end{bmatrix}$. This particular control design formulation is called the state-feedback (SF) problem [22]. For a given pre-specified $\gamma_c > 0$, to solve the H_∞ control problem of (5) with the specific SCC plant of (6), the controller parameters K_d, K_p, K_i can be obtained by the solution X of the Riccati equation [17] :

$$A_R^T X + XA_R - XBR_I^{-1}B^T X + \frac{C_1}{\gamma_c}^T (I - D_{1*}R_I^{-1}D_{1*}^T)\frac{C_1}{\gamma_c} = 0, \tag{7}$$

where

$$A_R = \left(A - BR_I^{-1}D_{1*}^T\frac{C_1}{\gamma_c}\right) \tag{8}$$

$$R_I = \frac{1}{\gamma_c^2}\begin{bmatrix} D_{12}^T D_{12} & D_{12}^T D_{11} \\ D_{11}^T D_{12} & -(\gamma_c^2 - D_{11}^T D_{11}) \end{bmatrix} \tag{9}$$

$$D_{1*} = \begin{bmatrix} \frac{D_{12}}{\gamma_c} & \frac{D_{11}}{\gamma_c} \end{bmatrix}, \quad B = \begin{bmatrix} B_2 & B_1 \end{bmatrix}. \tag{10}$$

Then, according to the control structure, the static H_∞ controller is given by

$$K_{c,\infty} = F_u = \begin{bmatrix} -K_d & -K_p & K_i \end{bmatrix}, \tag{11}$$

where

$$\begin{bmatrix} F_u \\ F_w \end{bmatrix} = -R_I^{-1}(B^T X + D_{1*}^T \frac{C_1}{\gamma_c}). \tag{12}$$

Now from (3), (6), and (11), the closed-loop system from $w = \begin{bmatrix} \omega^* & T_d \end{bmatrix}$ to $z = \begin{bmatrix} e_p^\# & e_\omega^\# & V^\# \end{bmatrix}^T$ can be found as

$$\begin{cases} \dot{x} = (A + B_2F_u)\,x + B_1 w \\ z = \left(\frac{C_1}{\gamma_c} + \frac{D_{12}}{\gamma_c}F_u\right)x + \frac{D_{11}}{\gamma_c}w, \end{cases} \tag{13}$$

where

$$A + B_2F_u = \begin{bmatrix} \frac{-K_d - R}{L} & \frac{-K_p - K_e}{L} & \frac{K_i}{L} \\ \frac{K_t}{J_m} & -\frac{B_m}{J_m} & 0 \\ 0 & -1 & 0 \end{bmatrix}. \tag{14}$$

By H_∞ control, which will ensure the stability of the closed-loop system, the eigenvalues of $A + B_2F_u$ are located in the left-half plane.

The corresponding input/output relationships between Figs. 5 and 7 are given by $w = \begin{bmatrix} \omega^* & T_d \end{bmatrix}$, $u = u_c$, $y = \begin{bmatrix} y_1 & y_2 & y_3 \end{bmatrix}^T$, and $z = \begin{bmatrix} e_p^\# & e_\omega^\# & V^\# \end{bmatrix}^T$. Since e_p is the position error, e_ω is the velocity error, and V is voltage in Fig. 7, the performance index formulation of the sub-optimal design is required to unify all of the dimensions. Here, the scaling factors of d_1, d_2 and d_3 are given, for example, by motor specifications, to nondimensionalize e_p, e_ω, and V into $\bar{e}_p$, $\bar{e}_\omega$, $\bar{V}$. Moreover, the constant weights α_1, α_2, and α_3 are employed for tuning the required performance in the proposed design process.

A procedure of weighting function selection is given in Fig. 8. First of all, the dimensions of transfer functions in the performance index of (4) should be unified by the scaling factors of d_1, d_2, and d_3 in accordance with the controlled motor specifications such that the infinity norm of each transfer function can be smaller than γ simultaneously. When the dimensionless parameters α_1, α_2, and α_3 are equal to one, the resulting control performance will be referred to as the basic design. Generally speaking, the basic design is given for further improvement in the control performance tuning. For ease of tuning, weights can be altered one at a time based on the relationship between control performance and its weights. Meanwhile, the controller parameters K_d, K_p and K_i are obtained by (6) to (12). Then, the closed-loop system poles can be calculated from (14) to ensure the stability of the closed-loop system. Repeat this simple tuning procedure until the desired control performance is achieved. It is known that the infinity norm of each transfer function of $e_p^\#/\omega^*$, $e_\omega^\#/\omega^*$ and $V^\#/\omega^*$ should be smaller than γ simultaneously owing to the control design of (4).

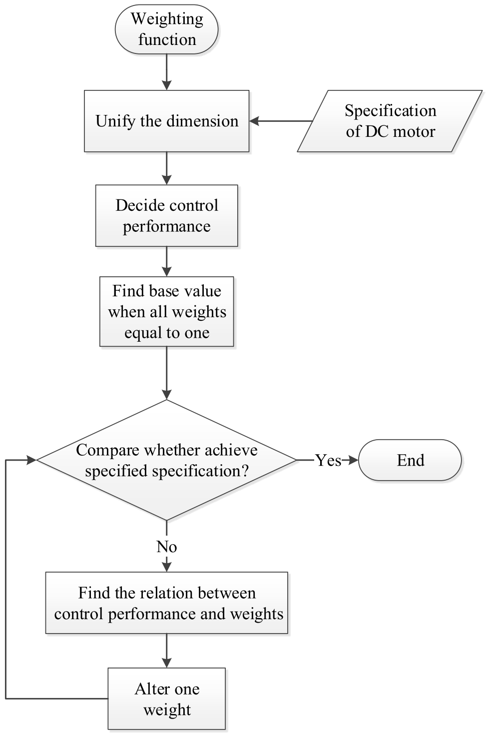

FIGURE 8. Flowchart of weighting function selection.

By motor specifications shown in Table 1, let W_p, W_ω and W_V be given by

$$W_p = \frac{\alpha_1}{d_1} = \frac{\alpha_1}{0.34/54.993(rad)} \tag{15}$$

$$W_\omega = \frac{\alpha_2}{d_2} = \frac{\alpha_2}{3000 \times \frac{2\pi}{60} \times 0.05(rad/s)}, \tag{16}$$

$$W_V = \frac{\alpha_3}{d_3} = \frac{\alpha_3}{75(volt)} \tag{17}$$

where $d_1 = 0.34/54.993(rad)$ is chosen to nondimensionalize position error e_p with respect to the stiffness K_{stiff} at the rated torque T_R; $d_2 = 3000 \times \frac{2\pi}{60} \times 0.05(rad/s)$ is to nondimensionalize e_ω with respect to the required velocity error 5% at the rated speed ω_R; $d_3 = 75(volt)$ is to

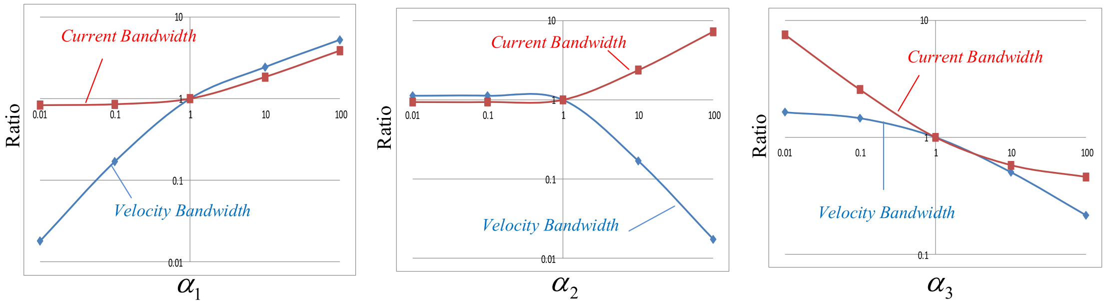

FIGURE 9. **Relationship between bandwidths and weights (α_1, α_2, α_3).**

nondimensionalize V with respect to the rated voltage V_R. Then, in letting $\alpha_1 = \alpha_2 = \alpha_3 = 1$ for an initial design, solving the H_∞ control design problem of (7) to (12) with a pre-specified $\gamma_c = 2$ can obtain a stabilizing controller $K_{c,\infty} = \begin{bmatrix} -K_d & -K_p & K_i \end{bmatrix}$ for which the resulting velocity bandwidth 160.52Hz and the current bandwidth 682.52Hz will be referred to as the basic design. According to the procedure of Fig. 8, weights of α_1, α_2, and α_3 should be chosen iteratively, as shown in the following, in order to illustrate the effectiveness of the proposed robust control design.

Note that the current-loop and velocity-loop bandwidths resulting from the classical cascaded design given above are the reference for control performance comparison. The relationships between the ratio of bandwidths and weights α_1, α_2, and α_3 are shown in Fig. 9,where the x-axis and y-axis denote the corresponding weight α_i and the ratio of the bandwidth with respect to the basic design, respectively (i.e., defined as the resulting bandwidth divided by the bandwidth of the basic design). As can be seen from Fig. 9, both current-loop and velocity-loop bandwidths can be enhanced by increasing α_1 while $\alpha_2 = \alpha_3 = 1$, while and only the current-loop bandwidth will be enhanced for $\alpha_1 = \alpha_3 = 1$ if α_2 is greater than 1. In addition, by increasing α_3 when $\alpha_1 = \alpha_2 = 1$, both the current-loop and velocity-loop bandwidths will be reduced. For example, let the bandwidth of the current loop be 1 kHz and the velocity bandwidth be 100 Hz. To obtain the desired control performances, α_2 is increased firstly from 1 to 3. According to the relationship between the bandwidths and α_2 as depicted in Fig. 9, the current-loop bandwidth resulting from the H_∞ PID-like design is found to be around 980 Hz, while the velocity-loop bandwidth is only 77 Hz. Next, if α_1 is further increased to 1.3 such that the current-loop and velocity-loop bandwidths are 992 Hz and 98 Hz, respectively, the H_∞ controller can be found by solving (7) to (12) with $\gamma_c = 2$ to be $K_i = 11936$, $K_p = 15.523$, and $K_d = 13.678$. Moreover, from (14), the closed-loop system poles are obtained as -1171.1, $-2187.4 \pm 2334.2i$, which verify the closed-loop system is stable. The resulting control performance approaches are compared to that of the classical cascade design. The current-loop and velocity-loop bandwidths of classical cascaded design and H_∞ PID-like control design are depicted in Fig. 10 and Fig. 11, respectively. Note that the overall weighting functions are given by $W_p = 210.27$, $W_\omega = 0.19099$, and $W_V = 0.0133$, which are chosen purposely to approximate to that of the classical cascade design.

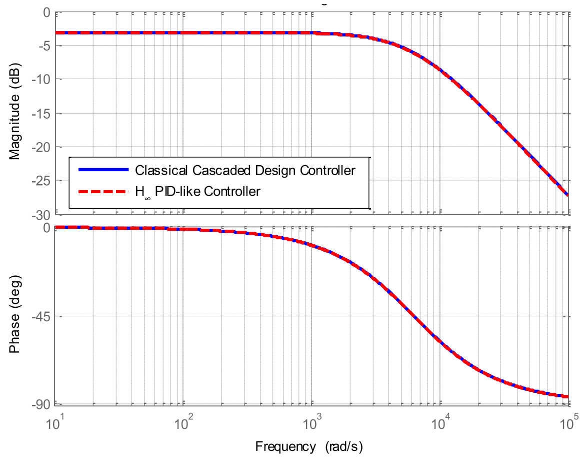

FIGURE 10. **Bode plot of current loop from i^* to i.**

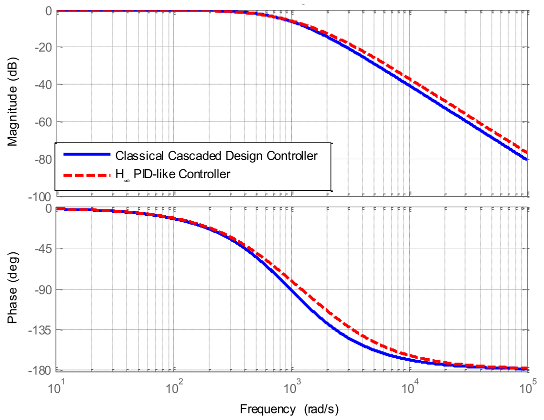

FIGURE 11. **Bode plot of velocity loop from ω^* to ω.**

For the velocity command of $\omega^* = 1500rpm$ in the servo control of Fig. 7, Fig. 12 shows that the step responses are close, resulting from the two designed controllers.

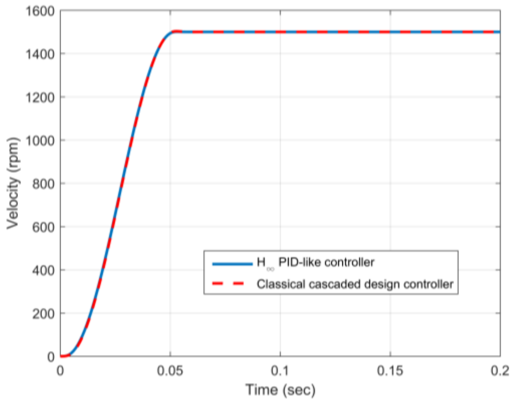

FIGURE 12. Time step response of velocity control.

Disturbance rejection ability, known as *dynamic stiffness*, is also an important performance index to evaluate the above servo controller design. Let the dynamic stiffness be characterized by the inverse magnitude of the closed-loop transfer function from the load torque disturbance T_d to the output speed ω. Fig. 13 shows the Bode plots of the dynamic stiffness, which concludes that the dynamic stiffness resulting from the H_∞ PID-like controller is superior to that of the classical cascade design.

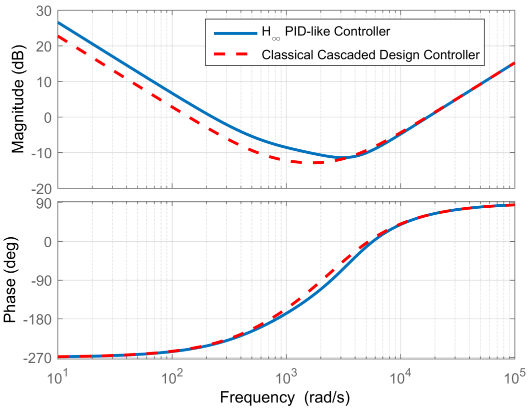

FIGURE 13. Bode plots of dynamic stiffness from velocity ω to torque T_d.

C. PROPOSED METHOD: H_∞ SPEED OBSERVER DESIGN

In practice, speed and current sensor noises, which lead to unwanted perturbations in control performance, will always exist, and the low-pass filter is commonly adopted for reducing sensor noise. However, the low-pass filter implemented in the feedback control loop will naturally cause phase-lag, which affects the stability margin. Observer design is a useful approach to overcoming the phase-lag problem in the feedback control. The speed observer design proposed in [18] is employed as shown in Fig. 14, which features high and low frequency paths, respectively, where the standard observed state $\hat{\omega}$ is constructed by the sum of the high and low frequency paths. To reduce the sensitivity of the senor noise and its phase delay problem simultaneously [18], the modified state $\hat{\omega}_{\mathrm{MOD}}$, coming from the low frequency path, is adopted for feedback control. Note that the motor involved in the observer design is modeled by the first-order system of $\frac{\hat{K}_t}{\hat{J}_m s+\hat{B}_m}$; the speed sensor model including a tachometer and a low-pass filter is regarded as the first-order filter with the cut-off frequency $\omega_c = 2\pi \times 100$ due to that the bandwidth of the low-pass filter is much less than the tachometer; the power amplifier is simplified as constant gain K_{amp} since its bandwidth is much greater than the current-loop bandwidth.

In addition to the PID-like controller design in Fig. 7, consider the robust observer design depicted in Fig. 15, where $W_{\omega m} = c_1\beta_1$, $W_i = c_2\beta_2$ and $W_n = c_3\beta_3$ shown in the dashed line are the input weighting functions to be selected for achieving the desired performance. The stabilizing observer compensator $K_{o,\infty} = \left[K_{do}\ K_{po}\ K_{io}\right]^T$ can be solved such that the infinity norm of the transfer functions from $i^\#$, $\omega^\#$, and $n^\#$ to e are smaller than a pre-specified γ_o. Since the input physical dimensions of the transfer functions e/i, e/ω, and e/n are all different, the dimensionless signals of $i^\#$, $\omega^\#$, and $n^\#$ are proposed here in the observer design, where c_1, c_2 and c_3 are from the given motor specifications to dimensionalize i, ω, and n, respectively, and the dimensionless constant weights β_1, β_2 and β_3 are design freedoms that can be employed to characterize the required control performances.

Similar to the SF control design formulation, let P_o denote the SCC plant from $\left[i^\#\ \omega^\#\ n^\#\right]$ to e for the speed observer design, where the state-space realization of $P_o(s)$ can be found from Fig. 15 as (18), as shown at the bottom of the next page.

Moreover, the H_∞ design problem is to find a stabilizing observer compensator, denoted $K_{o,\infty} = \left[K_{do}\ K_{po}\ K_{io}\right]^T$ [21] such that (4) is satisfied. As can been seen from $P_o(s)$ given in (18), the proposed observer design formulation is the output injection (OI) problem since $\hat{B}_2 = I$ and $\hat{D}_{12} = 0$ [22]. The H_∞ control solution of the OI problem is a dual case of the SF design. Dually, for a given pre-specified $\gamma_o > 0$, the static observer compensator can be solved by the solution Y of the Riccati equation [17]

$$\begin{aligned} &A_{R,o}^T Y + Y A_{R,o} - Y\hat{C}^T\tilde{R}_{II}^{-1}\hat{C}Y + \hat{B}_1(I - \hat{D}_{*1}^T\tilde{R}_{II}^{-1}\hat{D}_{*1})\hat{B}_1^T \\ &\quad = 0 \end{aligned} \tag{19}$$

$$A_{R,o} = \hat{A} - \hat{B}_1\hat{D}_{*1}^T\tilde{R}_{II}^{-1}\hat{C} \tag{20}$$

$$\tilde{R}_{II} = \begin{bmatrix} -\left(I - \dfrac{\hat{D}_{11}\hat{D}_{11}^T}{\gamma_o^2}\right) & \dfrac{\hat{D}_{11}\hat{D}_{21}^T}{\gamma_o} \\ \dfrac{\hat{D}_{21}\hat{D}_{11}^T}{\gamma_o} & \hat{D}_{21}\hat{D}_{21}^T \end{bmatrix} \tag{21}$$

$$\hat{D}_{*1} = \begin{bmatrix} \dfrac{\hat{D}_{11}}{\gamma_o} \\ \hat{D}_{21} \end{bmatrix}, \quad \hat{C} = \begin{bmatrix} \dfrac{\hat{C}_1}{\gamma_o} & \hat{C}_2 \end{bmatrix} \tag{22}$$

Then, the static controller is given by

$$K_{o,\infty} = H_y = \begin{bmatrix} K_{do} & K_{po} & K_{io} \end{bmatrix}, \tag{23}$$

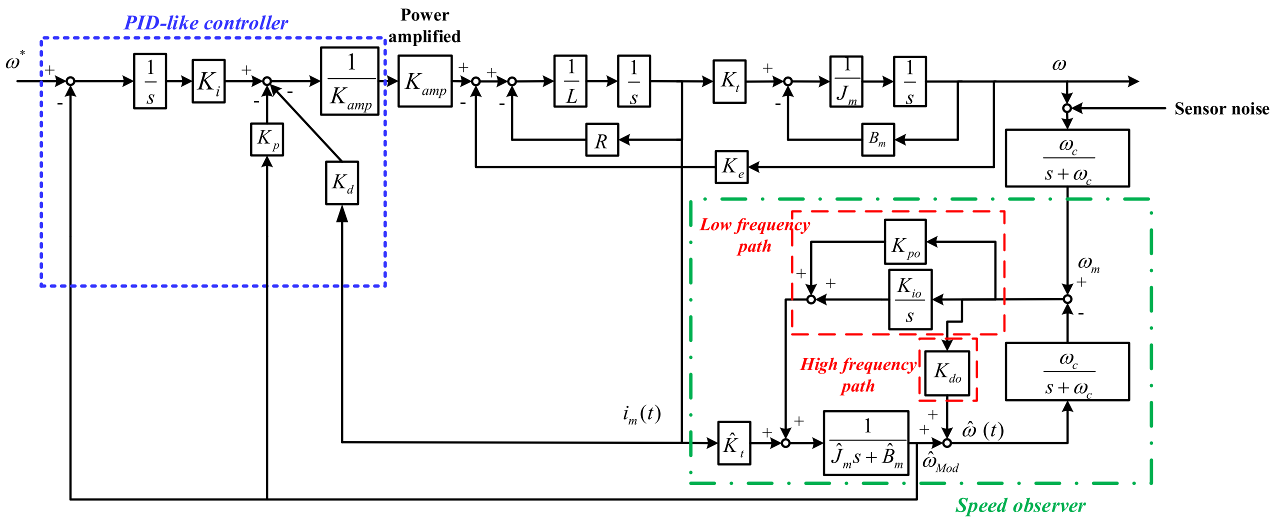

FIGURE 14. Block diagram of DC motor controlled by PID-like controller with speed observer.

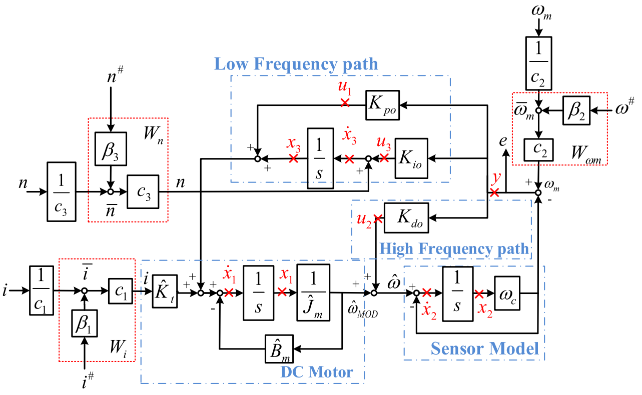

FIGURE 15. Speed observer of the DC motor.

where

$$\begin{bmatrix} H_u \\ H_y \end{bmatrix}^T = -(Y\hat{C}^T + \hat{B}_1\hat{D}_{*1}^T)\tilde{R}_{II}^{-1}. \tag{24}$$

The speed observer from $w_o = \begin{bmatrix} i^\# & \omega^\# & n^\# \end{bmatrix}$ to $z_o = e$ can be formulated from (3), (18) and (23) as

$$\begin{cases} \dot{x} = \left(\hat{A} + H_y\hat{C}_2\right)x + \hat{B}_1 w_o \\ z_o = \dfrac{\hat{C}_1}{\gamma_o}x + \dfrac{\hat{D}_{11}}{\gamma_o}w_o. \end{cases} \tag{25}$$

where

$$\hat{A} + H_y\hat{C}_2 = \begin{bmatrix} -\dfrac{\hat{B}_m}{\hat{J}_m} & -K_{do}\omega_c & 1 \\ \dfrac{1}{\hat{J}_m} & -\left(1+K_{po}\right)\omega_c & 0 \\ 0 & -K_{io}\omega_c & 0 \end{bmatrix}. \tag{26}$$

Note that the eigenvalues of $\hat{A} + H_y\hat{C}_2$ must be located at the left-half plane to ensure the stability of the speed observer.

In order to properly choose the weighting functions W_i, $W_{\omega m}$, and W_n depicted in Fig. 15 for characterizing the required performance, consider the specifications of the controlled motor shown in Table 1, and W_i, $W_{\omega m}$ and W_n be given by

$$W_i = \beta_1 \times c_1 = \beta_1 \times 2(A) \tag{27}$$

$$W_{\omega m} = \beta_2 \times c_2 = \beta_2 \times 3000 \times \frac{2\pi}{60}(\text{rad/s}) \tag{28}$$

$$W_n = \beta_3 \times c_3 = \beta_3 \times \frac{3400}{3000 \times \frac{2\pi}{60}}(N \cdot m/s), \tag{29}$$

$$P_o(s) \overset{s}{=} \left[\begin{array}{c|cc} \hat{A} & \hat{B}_1 & \hat{B}_2 \\ \hline \hat{C}_1 & \hat{D}_{11} & \hat{D}_{12} \\ \hat{C}_2 & \hat{D}_{21} & 0 \end{array}\right] = \left[\begin{array}{ccc|ccc:ccc} -\dfrac{\hat{B}_m}{\hat{J}_m} & 0 & 1 & W_i\hat{K}_t & 0 & 0 & 1 & 0 & 0 \\ \dfrac{1}{\hat{J}_m} & -\omega_c & 0 & 0 & 0 & 0 & 0 & 1 & 0 \\ 0 & 0 & 0 & 0 & 0 & W_n & 0 & 0 & 1 \\ \hline 0 & -\omega_c & 0 & 0 & W_{\omega m} & 0 & 0 & 0 & 0 \\ \hdashline 0 & -\omega_c & 0 & 0 & W_{\omega m} & 0 & 0 & 0 & 0 \end{array}\right] \tag{18}$$

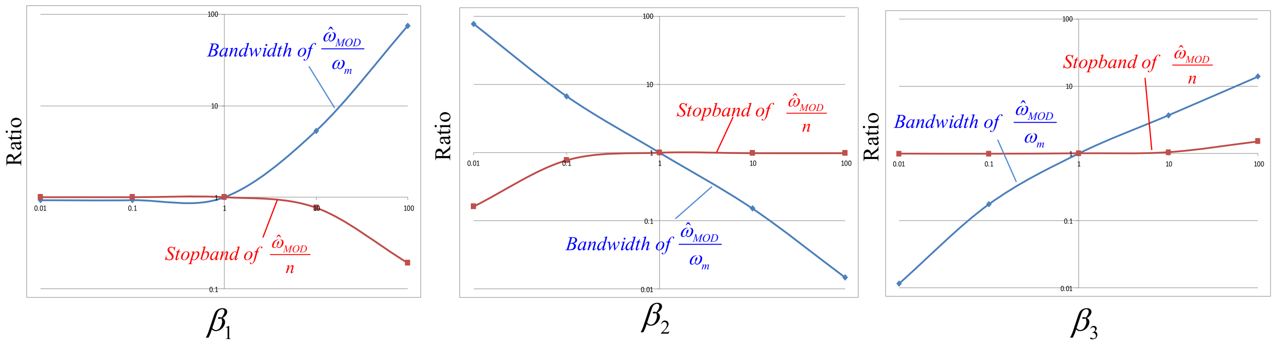

FIGURE 16. Relationships among weights β_1, β_2, and β_3.

where $c_1 = 2(A)$ is from the motor rated current i_R; $c_2 = 3000 \times \frac{2\pi}{60}$(rad/s) is from the motor rated speed ω_R; $c_3 = \frac{3400}{3000\times\frac{2\pi}{60}}$ comes from the derivative of torque; which is defined by the power rate $\dot{P}_R$ divided by the rated speed ω_R.

Observer bandwidth is the key specification to be considered. Besides, an observer is also susceptible to noise, thus making noise another important consideration. In fact, noise can be classified as command noise, calculation noise, or sensor noise based on the noise entry points [24]. In this paper, the effect of command noise and sensor noise on the observer design can be neglected due to the low-pass filter in our control system. However, the calculation noise n as shown in Fig. 15 is still a problem to the observer design. In order to clarify the ability of noise immunity, the stopband bandwidth of noise sensitivity, defined as a frequency that disallows noise to pass [25], is another specification to be considered when designing an observer. In letting $\beta_1 = \beta_2 = \beta_3 = 1$ in (27), (28), and (29) for an initial design, solving the H_∞ control design problem of (4) with the SCC plant P_o given by (18) and $\gamma_o = 2$ will obtain $K_{o,\infty} = \left[K_{do}\ K_{po}\ K_{io}\right]^T$ for which the resulting observer bandwidth 6.7916 Hz and the stopband bandwidth of calculation noise sensitivity 25.4 Hz will be referred to as the basic design. Similar to the design procedure of Fig. 8, the weights of β_1, β_2 and β_3 can be selected iteratively in order to achieve the desired performance, which is, in terms of noise sensitivity, a 100Hz speed observer bandwidth and a 10Hz stopband bandwidth. The relationship between the different weights β_1, β_2, β_3 and the resulting performance are depicted in Fig. 16, where the x-axis and y-axis denote the weights β_1, β_2, β_3 and the ratio of resulting bandwidth, which is divided by that of the basic design, respectively. Firstly, β_3 increases from 1 to 100 based on Fig. 16; the speed observer bandwidth resulting from the H_∞ PID-like design is 95.177 Hz, which approaches the desired observer bandwidth, while the stopband bandwidth of the noise sensitivity is 38.579Hz. Next, β_1 increases from 1 to 37 such that the stopband bandwidth of noise sensitivity reduces to 11.053 Hz, which is near the desired stopband bandwidth for noise sensitivity; however, the speed observer bandwidth is enhanced to 210.21 Hz. Thus, by increasing β_2 from 1 to 2.1, the resulting bandwidths of the speed observer and noise sensitivity are 101.48 Hz and 10.95 Hz, respectively, which are close to the desired performance. Moreover, the poles of the speed observer are obtained from (26) as $-70.7, -473.12 \pm 170i$, which verify that the speed observer is stable. Note that the compensator of the speed observer can be obtained as $K_{io} = 1.6404$, $K_{po} = 0.02847$, and $K_{do} = 0.6033$ by solving (19) to (24). The simulation result of Fig. 14 is depicted in Fig. 17, which shows that the velocity from the speed observer ω_{mod} has effectively reduced the phase delay problem that comes from the low-pass filter.

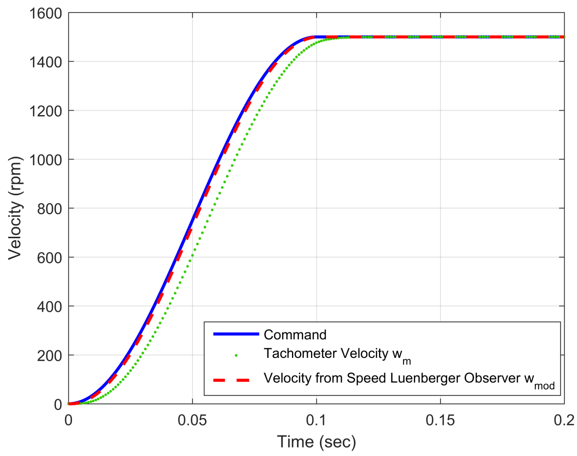

FIGURE 17. Velocity step response with speed observer.

Due to the external load and/or the parameter inaccuracy, the inertia of a servo control system often varies in practice during operations. The variation of parameter J_m, which is often away from its nominal value $J_o = 5.77 \times 10^{-5} kg \cdot m^2$, will lead to the significant alteration in its output response of speed control. To illustrate the effect of model uncertainties, three cases of $J_m = 0.5J_o$, $J_m = J_o$ and $J_m = 2J_o$ are respectively investigated by computer simulations. Fig. 18 shows the velocity step response with model uncertainty J_m. As can be seen, the velocity response resulting from $J_m = 2J_o$ and $J_m = 0.5J_o$ are almost the same as that of $J_m = J_o$. Furthermore, the effect of parameter variations of damping

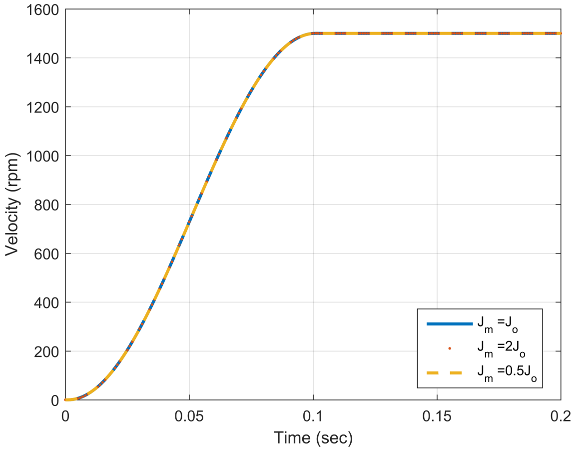

FIGURE 18. Velocity step response with model uncertainty J_m.

coefficient B_m is also discussed in the case of $B_m = 4B_o$ and $J_m = 2\ J_o$. Fig. 19 shows the velocity step response with model uncertainty J_m and B_m; the resulting responses are close.

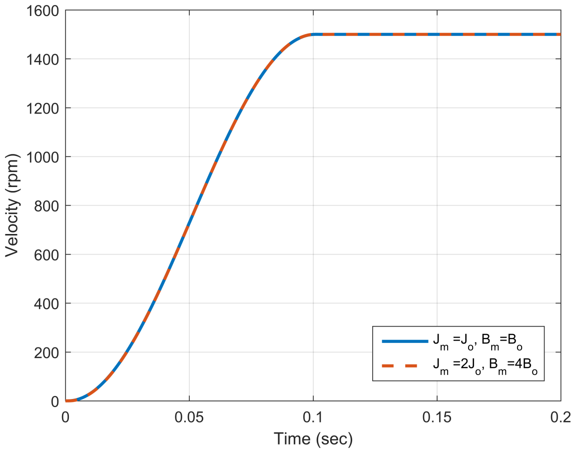

FIGURE 19. Velocity step response with mechanical model uncertainty.

III. EXPERIMENTAL SETUP AND RESULTS

A mechanical experimental setup is shown in Fig. 20 (a), where the controlled plant is a DC servomotor (110W rated power output), whereas the overall concept for controlling and data capturing is shown in Fig. 20 (b). In order to validate the theoretical results, the robust PID-like controller and speed observer are implemented by a DSP real-time controller as depicted in Fig. 20 (b), where the current and velocity signals are measured by a current-meter and tachometer (minimum speed measurement is 8.75rpm), respectively. A Compact RIO Controller (cRIO-9031) [26] with a 16-Bit resolution of ADC and DAC and the amplifier module NF-HSA4052 are utilized to drive the DC servomotor. Moreover, the feedback controller and speed observer designed in Section II, discretized by the bilinear method [27], are implemented in the Compact RIO Controller with a sampling frequency of 10kHz. For validating the ability of the proposed design to reject disturbances, a loading motor is given to generate the required mechanical torque disturbance for performance evaluation.

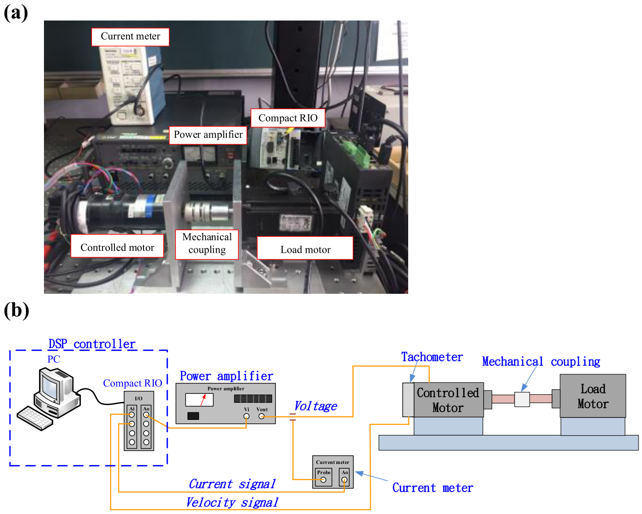

FIGURE 20. Experimental system.

In order to characterize the proposed speed observer, the DC brush motor is driven by a robust PID-like controller and speed observer without the coupling servo motor. Fig. 21 presents a comparison of experiment results measured from the tachometer and speed observer, respectively. Measuring the velocity measured from the tachometer (dashed line in Fig. 21) reveals the phase delay problem caused by the low-pass filter, while the proposed speed observer has effectively reduced the phase delay problem as the dotted line depicted in Fig. 21. A comparison of current response from simulation and experiment, respectively, are depicted in Fig. 22. Obviously, the maximum of the current response is 0.9 (A), which is bounded in the specification of rated current 2 (A).

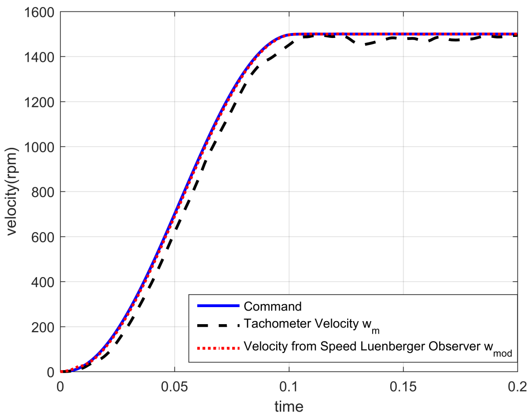

FIGURE 21. Time step response with speed observer.

To illustrate the effect of parameter uncertainties, two set of test experiments are performed:

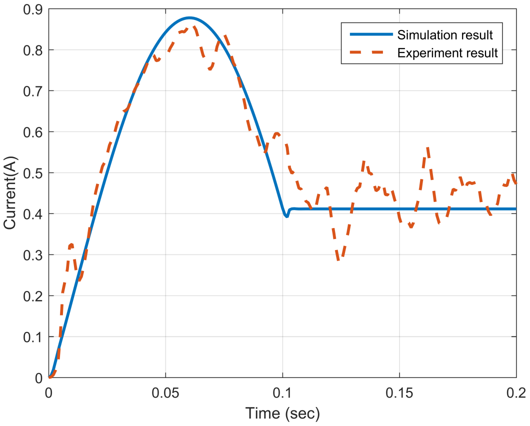

FIGURE 22. **Dynamic response of current.**

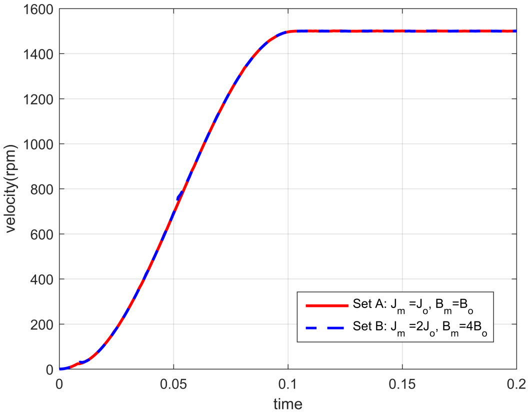

FIGURE 23. **Velocity step response with mechanical model uncertainty.**

Set A. The DC servomotor is controlled by the proposed PID-like controller and speed observer without coupling to the external loading motor.

The DC servomotor coupled with the loading motor is controlled by the proposed PID-like controller and speed observer, the same as Set A.

Since the torsional stiffness of the mechanical coupling shown in Fig. 20 (a) is high enough as a rigid body, the total inertia J_m and damping coefficient B_m in Set B are given by

$$J_m = J_o + J_L \tag{30}$$

$$B_m = B_o + B_L, \tag{31}$$

wher $J_o = 5.77 \times 10^{-5} kg \cdot m^2$ and $B_o = 0.00055\ N \cdot m \cdot s/rad$ are the inertia and damping coefficient of the DC servomotor, respectively; $J_L = 6.8 \times 10^{-5} kg \cdot m^2$ and $B_L = 0.002\ N \cdot m \cdot s/rad$ are the inertia and damping coefficient of the loading motor, respectively. Note that the total inertia and damping coefficient of Set B are $J_m \approx 2J_o$, $B_m \approx 4B_o$, respectively. Fig. 23 depicts the measured velocity results from experimental tests of Set A and Set B, respectively. It is evident that the velocity response resulting from $J_m \approx 2J_o, B_m \approx 4B_o$ is almost the same as that of $J_m = J_o, B_m = B_o$, which is identical to the simulation result as shown in Fig. 19, verifying the robustness of the proposed control performance.

To verify the ability of the proposed method to reject disturbances, the measured velocity resulting from the H_∞ PID-like controller and the classical cascade design controller, respectively, are depicted in Fig. 24 with an overall execution time of 10 seconds, where a step torque 0.3 Nm causes a disturbance at 3 seconds. According to Fig. 24 (a) and (b), a large oscillation of the velocity is

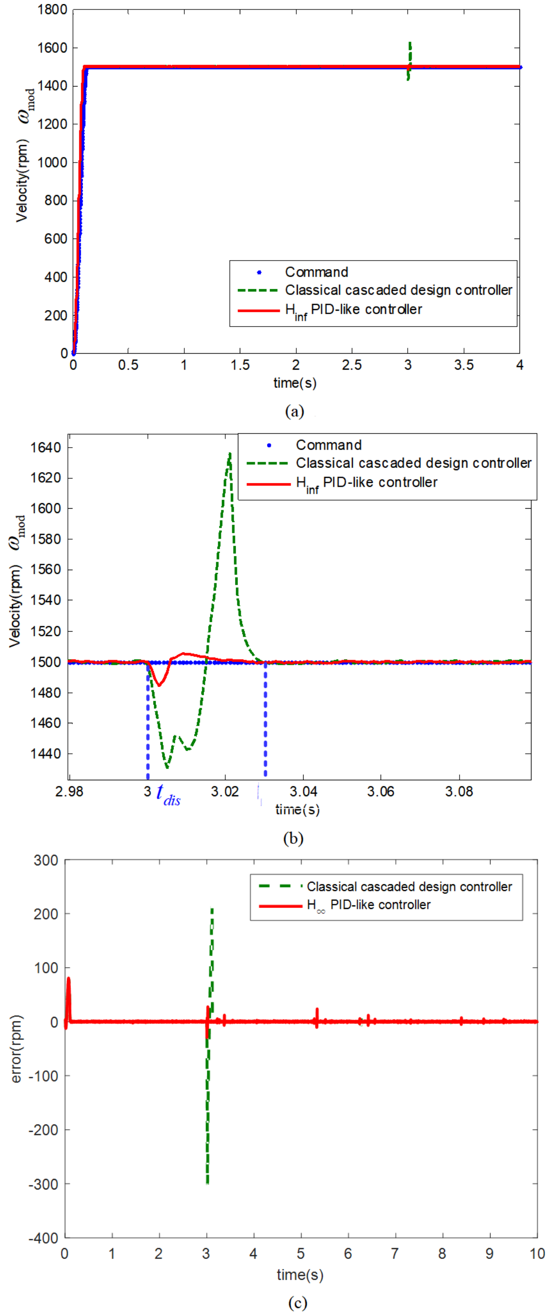

(a)

(b)

(c)

FIGURE 24. **Measurement velocity results with 0.3 Nm disturbance torque. (a) Velocity step response disturbing at 3 seconds. (b) Zoom-in of velocity step response disturbing at 3 seconds. (c) Tracking errors of velocity step response.**

apparent and is caused when the DC servomotor is driven by a classical cascade design controller. However, the oscillation of the velocity, measured from the DC servomotor driven by the H_∞ PID-like controller, becomes much smaller, which can also be verified in Fig 24 (c). The corresponding current and voltage signals are illustrated as Figs. 25 and 26, respectively.

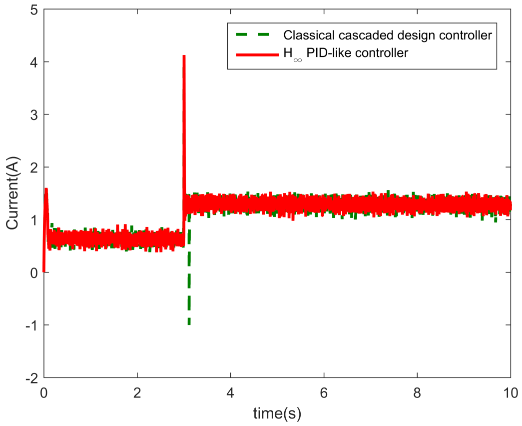

FIGURE 25. **Current signals with 0.3 Nm disturbance torque.**

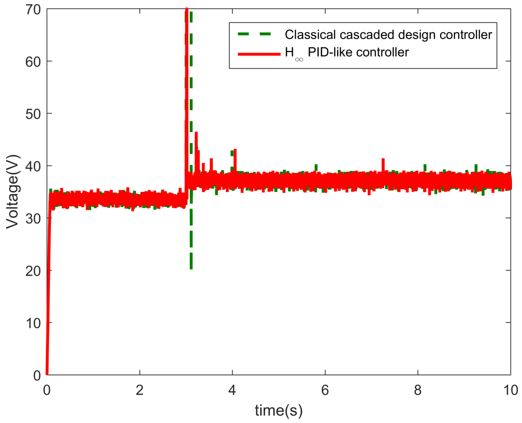

FIGURE 26. **Voltage signals with 0.3 Nm disturbance torque.**

To clarify the disturbance rejection, the maximum tracking errors, standard deviations of the tracking errors, and recovery time t_r are determined as exemplarily. Note that the recovery time t_r is

$$t_r = t_s - t_{dis}, \tag{32}$$

where t_{dis} is the time when the disturbance torque disrupts the system; t_s is the time it takes the velocity to recover to steady velocity after the disturbance torque disturbs the system. Notice that the maximum tracking errors, standard deviations of the tracking errors, and recovery time are significantly decreased as illustrated in Table 2. Consequently, the proposed H_∞ PID-like controller is superior to that of the classical cascade design, which has also been confirmed in the simulation results shown in Fig. 13.

TABLE 2. **Results of 0.3 Nm disturbance torque.**

	Maximum tracking error (rpm)	Standard deviations of tracking error (rpm)	Recovery time (s)
Classical design controller	214.1751	15.683	0.122
H_∞ PID-like controller	27.5437	1.1179	0.033

IV. CONCLUSION

This paper has presented a PID-like controller structure and a speed observer for a servo drive, and special H_∞ control synthesis (i.e., SF case and OI case) is formulated respectively such that the controller parameters and the observer compensator can be obtained directly. In addition, the weighting function selection based on the motor specifications is given to form a basic design, and then relative constant weights are selected iteratively to provide for further performance improvement. Finally, the proposed controller design was experimentally implemented in a DC servomotor system to verify the control performance. The experiment results show that the proposed H_∞ PID-like controller is superior to that of the classical cascaded design in terms of rejecting disturbances. Moreover, the proposed speed observer has effectively reduced the phase delay problem.

ACKNOWLEDGMENT

The authors are grateful to Mr. Ming-Wei Shen who contributed to pre-research of this study, and the authors would like to thank the anonymous reviewers for their valuable suggestions, which led to significant improvements of this paper.

REFERENCES

[1] H. Zhou, "DC servo motor PID control in mobile robots with embedded DSP," in *Proc. Int. Conf. Intell. Comput. Technol. Automat.*, 2008, pp. 332–336.
[2] K. Newton, W. Steeds, and T. K. Garrett, *The Motor Vehicle*. London, U.K.: Butterworth, 1983.
[3] K. Osakada, K. Mori, T. Altan, and P. Groche, "Mechanical servo press technology for metal forming," *CIRP Ann.-Manuf. Technol.*, vol. 60, no. 2, pp. 651–672, 2011.
[4] T.-K. Liu, D. H. Al-Janan, H.-S. Shen, and P.-W. Hsueh, "Optimizing adjustable parameters of servo controller by using UniNeuro-HUDGA for laser-auto-focus-based tracking system," *IEEE Access*, vol. 5, pp. 823–832, 2017.
[5] G. Ellis, *Control System Design Guide: Using Your Computer to Develop and Diagnose Feedback Controllers*. San Diego, CA, USA: Academic, 1991.
[6] C.-J. Hsu and Y.-S. Lai, "Novel on-line optimal bandwidth search and auto tuning techniques for servo motor drives," in *Proc. IEEE Energy Convers. Congr. Expo. (ECCE)*, Sep. 2016, pp. 1–8.
[7] M. A. Johnson and M. H. Moradi, *PID Control: New Identification and Design Methods*. London, U.K.: Springer-Verlag, 2005.
[8] O. D. I. Nwokah, "Pseudo-derivative feedback control," in *Proc. Amer. Control Conf.*, 1987, pp. 1811–1814.
[9] K. H. Ang, G. Chong, and Y. Li, "PID control system analysis, design, and technology," *IEEE Trans. Control Syst. Technol.*, vol. 13, no. 4, pp. 559–579, Jul. 2005.
[10] J. G. Ziegler and N. B. Nichols, "Optimum settings for automatic controllers," *J. Dyn. Syst., Meas.*, vol. 115, pp. 220–222, Jun. 1993.

[11] J.-B. He, Q.-G. Wang, and T.-H. Lee, "PI/PID controller tuning via LQR approach," *Chem. Eng. Sci.*, vol. 55, pp. 2429–2439, Jul. 2000.
[12] K. Li, "PID tuning for optimal closed-loop performance with specified gain and phase margins," *IEEE Trans. Control Syst. Technol.*, vol. 21, no. 3, pp. 1024–1030, May 2013.
[13] A. Dai, X. Zhou, and X. Liu, "Design and simulation of a genetically optimized fuzzy immune PID controller for a novel grain dryer," *IEEE Access*, vol. 5, pp. 14981–14990, Jul. 2017.
[14] H. Yan, X. Wang, G. Duan, and T. Zhao, "Application of H_∞ robust control algorithm to a precision linear motor displacement system," *J. Tsinghua Univ. (Sci. Technol.)*, vol. 46, no. 11, pp. 1828–1831, 2006.
[15] X. Zhao and Q. Guo, "Robust control based on internal model theory for linear permanent magnet synchronous motor," in *Proc. Elect. Mach. Syst.*, 2005, pp. 1613–1616.
[16] S. Liu, X. Guo, and L. Zhang, "Robust adaptive backstepping sliding mode control for six-phase permanent magnet synchronous motor using recurrent wavelet fuzzy neural network," *IEEE Access*, vol. 5, pp. 14502–14515, Jun. 2017.
[17] M. C. Tsai and D. W. Gu, *Robust and Optimal Control: A Two-Port Framework Approach*. London, U.K.: Springer-Verlag, 2014.
[18] G. Ellis, *Observer in Control Systems: A Practical Guide*. San Diego, CA, USA: Academic, 2002.
[19] H. Kimura, *Chain-Scattering Approach to H_∞ Control*. Boston, MA, USA: Birkhauser, 1997.
[20] D. C. McFarlane and K. Glover, *Robust Controller Design Using Normalized Coprime Factor Plant Descriptions*. London, U.K.: Springer-Verlag, 1990.
[21] K. Zhou, J. C. Doyle, and K. Glover, *Robust and Optimal Control*. Upper Saddle River, NJ, USA: Prentice-Hall, 1995.
[22] K. Zhou and J. C. Doyle, *Essentials of Robust Control*. Upper Saddle River, NJ, USA: Prentice-Hall, 1998.
[23] J. C. Doyle, K. Glover, P. P. Khargonekar, and B. A. Francis, "State-space solutions to standard H_2 and H_∞ control problems," *IEEE Trans. Autom. Control*, vol. 34, no. 8, pp. 831–847, Aug. 1989.
[24] G. Ellis, *Observer in Control Systems: A Practical Guide*. San Diego, CA, USA: Academic, 2002.
[25] "T. F. Schubert, Jr., and E. M. Kim, *Fundamentals of Electronics: Book 3 Active Filters and Amplifier Frequency Response*. San Rafael, CA, USA: Morgan & Claypool, 2016.
[26] Compact RIO. *National Instruments*. Accessed: May 2009. [Online]. Available: http://www.ni.com/white-paper/52251/en/
[27] P. Katz, *Digital Control Using Microprocessors*. Upper Saddle River, NJ, USA: Prentice-Hall, 1981.

PO-JEN KO (S'10) was born in Chiayi, Taiwan, in 1986. He received the B.Eng. degree in mechanical engineering from National Central University, Taiwan, in 2008, and the M.Sc. degree in mechanical engineering from National Cheng Kung University, Taiwan, in 2010. He is currently pursuing the Ph.D. degree with the Department of Mechanical Engineering, National Cheng Kung University, Tainan, Taiwan.

He has authored two published journal papers. He holds one U.S. patent. His current research interests include motion control, robust control, and electric motor diagnostics.

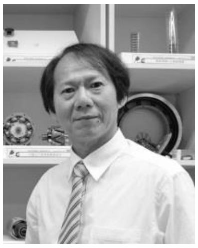

MI-CHING TSAI (S'87–M'89–SM'98) was born in Tainan, Taiwan, in 1956. He received the B.S. and M.S. degrees in electronic engineering from the National Taiwan University of Science and Technology, Taiwan, in 1981 and 1983, respectively, and the Ph.D. degree from the Department of Engineering Science, University of Oxford, Oxford, U.K., in 1990.

In 1996, he became a Full Professor with the Department of Mechanical Engineering, National Cheng Kung University, Tainan. From 2003 to 2004, he was also a Visiting Scholar with the Control Division, Department of Engineering, Cambridge University, Cambridge, U.K. From 2016 to 2017, he was appointed as the Deputy Minister of the Ministry of Science and Technology, Taiwan. He is currently a Chair Professor with National Cheng Kung University. He has authored or co-authored over 117 published refereed journal papers. He holds over 117 patents. His research interests include robust control, servo control, motor design, and applications of advanced control technologies using DSPs.

Dr. Tsai is a fellow of the Institution of Engineering and Technology, U.K. He was an Associate Editor of the IEEE/ASME Transactions on Mechatronics from 2003 to 2007.

• • •